Variability and Reproducibility of Rubidium-82 Kinetic Parameters in the Myocardium of the Anesthetized Canine

Pamela G. Coxson, Kathleen M. Brennan, Ronald H. Huesman, Sophanie Lim and Thomas F. Budinger

Center for Functional Imaging, Life Sciences Division, Lawrence Berkeley Laboratory, University of California, Berkeley, California

Kinetic analysis of ^{82}Rb dynamic PET data produces quantitative measures which could be used to evaluate ischemic heart disease. These measures have the potential to generate objective comparisons of different patients or the same patient at different times. To achieve this potential, it is essential to determine the variability and reproducibility of the kinetic parameters. **Methods:** A total of 48 ^{82}Rb dynamic PET datasets were acquired from two pure bred beagles. Each animal underwent eight ^{82}Rb PET studies with essentially the same protocol for three successive weeks. Data were acquired with the Donner 600-Crystal Positron Tomograph (PET600). In each week, single-slice dynamic ^{82}Rb PET datasets were collected with the animal at rest at three different gantry positions separated by 5 mm. Additional dataset were collected after dipyridamole infusion and after administration of aminophylline to induce a return to rest. A two-compartment kinetic model with correction for myocardial vasculature and spillover from the left ventricular blood pool was used to analyze the dynamic datasets. Model parameters for uptake (k_1), washout (k_2) and vascular fraction (f_v) were estimated in 11–14 myocardial regions of interest (ROIs) using a weighted least-squares criterion. Statistical fluctuation due to the PET acquisition process was minimized by using a relatively high ^{82}Rb dose (about 30 mCi) to take advantage of the high count rate capacity of the PET600. **Results:** The variation in mean k_1, where the mean is taken over the myocardial ROIs was 10%–20% (Dog 1) and 15%–50% (Dog 2) among the rest studies conducted on the same date. Similar variation was evident in comparing studies in the same animal for different weeks. **Conclusion:** Spatial and temporal variation in estimates of the uptake rate (k_1) of ^{82}Rb in the resting myocardium of the anesthetized canine are small in relation to the functional increase in k_1 following dipyridamole infusion.

Key Words: dynamic PET; rubidium-82; kinetic models; myocardium; dipyridamole stress

J Nucl Med 1995; 36:287–296

The use of ^{82}Rb with PET for evaluation of ischemic heart disease relies on visual examination of images before and during pharmacologically induced vasodilation (e.g., adenosine or dipyridamole infusion) (*1,2*). Kinetic analysis holds out the possibility of obtaining quantitative measures which can be used to make region-by-region comparisons of different patients or the same patient at different times (*3*). A variety of quantitative measures have been proposed (*4,5*). Validation has proceeded by comparison with microsphere measures of blood perfusion. Reproducibility of the quantitative measure has not been studied. Thus, we do not know whether the same result will be observed when the data are collected another time: later the same day or next week, for example. A clinical trial to determine the efficacy of kinetic analyses involves at the outset a determination of the variability and reproducibility of the quantitative measures. To the extent that we cannot anticipate all sources of variability, this issue must be resolved by replicate experiments in animals and human subjects.

We have carried out experiments designed to assess the reproducibility of the kinetic parameters for ^{82}Rb in the dog heart. A series of ^{82}Rb PET kinetic datasets were acquired with controlled changes in conditions: (1) the same sequence of measurements on three separate dates; (2) baseline measurements taken at three PET positions, separated by 5 mm; (3) three measurements in which the length of time taken to inject rubidium was varied (5 sec, 30 sec, 60 sec); (4) repeated measurements at the same position; and (5) a sequence of changes in state, i.e., at rest, with dipyridamole and returned to rest. The studies were carried out with two animals, using a total of 48 independent ^{82}Rb injection datasets. These data provide an indication of between animal variation, but the principal goal was to understand the variation in parameters and parameter estimates based on measurements taken from the same animal. Variability from counting statistics was minimized in order to isolate underlying physiological variability.

METHODS

Two pure-bred beagles underwent a series of ^{82}Rb PET studies with essentially the same protocol, in three successive weeks. Both dogs were of similar age and weight. Dog 1, a 17-kg male, was trim and muscular with a heart rate that averaged 100–110 bpm; Dog 2, an 18.5-kg female, was overweight and nonmuscular with a heart rate that averaged 120–140 bpm. The dogs were

positioned in right lateral recumbency and the left ventricle was imaged with ^{82}Rb from a generator (6) at three consecutive levels of 5 mm thickness. The position with a large, well-defined blood pool was selected from these three levels and all further imaging was at the same level using a single-layer, high-resolution PET scanner.

PET imaging was performed using the Donner 600-Crystal Positron Tomograph (7). The detector assembly consists of a single ring of 600 bismuth germanate (BGO) crystals, each 3 mm wide and individually coupled to a phototube. Stationary test results show in-plane resolution of 2.9 mm FWHM at the center of the gantry and an elliptical point spread function of 3.0 mm × 4.0 mm FWHM at 8 cm from the center of the gantry for a ^{22}Na wire source (8). Due to positron range effects, the resolution for ^{82}Rb is about 5 mm FWHM (based on measured value of 5.7 mm FWHM using a Butterworth filter with f_p, $f_s = 1, 3$ cycles/cm (9)). Resolution can be enhanced by either clamming (detectors alternated between interlacing angular positions, doubling the linear sampling frequency), or by gating to real time EKG measurements to reduce blurring due to heart motion. Hardware constraints do not allow both clamming and gating in the same dynamic study. In this series of studies, acquisitions were acquired with two gates. Slice thickness was fixed at 6 mm FWHM throughout this study. An orbiting-point positron (^{68}Ge) source with electronic masking reduces imaging time to 3 min per transverse section for transmission images and minimizes the scatter contribution (10). Dead time losses are minimal. With 60 mCi uniformly distributed in a 20-cm diameter by 0.5-cm thick water-filled phantom in the field of view, data were acquired with an estimated 4% dead time loss (Moses WW, personal communication). This tomograph has produced images with 200 mCi in the field of view (a single slice).

Anesthesia was induced with intravenous sodium thiamylal and maintained with methoxyflurane/N_2O/O_2 delivered via an Ohio Metamatic ventilator (Ohio Metamatic, Madison, WI). A polyethylene catheter was placed in the cephalic vein for injection and maintenance fluid administration. A femoral artery was catheterized and used for periodic blood gas analysis to maintain physiologically normal values over the duration of the study. EKG leads were attached and lead II was monitored continuously.

The basic protocol for the experiments called for a sequence of eight ^{82}Rb injections as shown in Figure 1. Vasodilation was induced by a 5-min infusion of dipyridamole (1.6 mg/kg) and was subsequently countered with an injection of aminophylline (2.3 mg/kg). The dipyridamole infusion was halted early if mean blood pressure dropped below 70 mmHg, in which case the administered dose was somewhat lower. For each ^{82}Rb injection, kinetic data were acquired over 6 min in 28 data files: sixteen 5-sec files, four 10-sec files, six 30-sec files and two 60-sec files.

For completeness, we describe in detail all deviations from the basic protocol: In Week 1, the protocol was followed for both animals. Technical difficulties caused a delay in starting the study with the second dog. The animal was under anesthetic for 2 hr before the first injection could be given. Once the injections had begun, there were no further delays. The last emission dataset (postaminophylline) for Dog 2 did not have a usable blood pool, so it had to be omitted from the kinetic analysis. In Weeks 2 and 3, the protocol was modified slightly to include a second bolus and measurement of ^{82}Rb after dipyridamole (and before aminophylline).
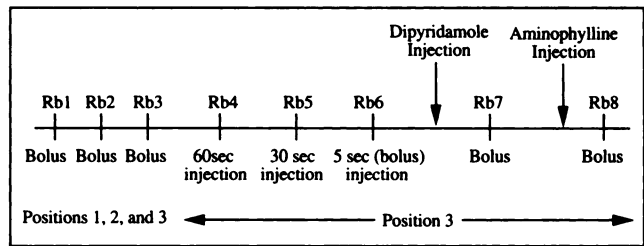

FIGURE 1. Experimental protocol. A sequence of eight dynamic PET datasets were collected to observe the myocardium in three distinct states: rest, dipyridamole and returned to rest (postaminophylline). The first three datasets (Rb1, Rb2, Rb3) were acquired at three different positions—lateral slices separated by 5 mm. The remaining data were collected at one of the three initial positions (denoted position 3).

Data Analysis

Kinetic Parameter Estimation. Each dynamic ^{82}Rb dataset was analyzed using a two-compartment model (Fig. 2) with correction for myocardial vasculature and spillover from the left ventricular blood pool:

$$y(t) = f_v u(t) + (1 - f_v)x(t)$$

$$= f_v u(t) + (1 - f_v) \int_0^t e^{-k_2(t-\tau)}k_1 u(\tau) \, d\tau,$$

where y(t) is the concentration of ^{82}Rb in the myocardial ROI; x(t) is the ^{82}Rb in the nonvascular component of the myocardial ROI; u(t) is the concentration of ^{82}Rb in the left ventricular blood pool; k_1 is the myocardial uptake rate (min^{-1}); k_2 is the washout rate (min^{-1}); and f_v is the vascular fraction.

The kinetic parameters k_1, k_2 and f_v and their variances were estimated from the 28 data files corresponding to the 28 time intervals in each dynamic PET dataset. Parameter estimates were determined to minimize a weighted least-squares criterion:

$$(Y - Y^*)^T \Phi^{-1}(Y - Y^*),$$

where $Y(U^*, k_1, k_2, f_v)$ is a vector whose i^{th} element, $i = 1, \ldots ,$ 28, is given by $y_i = \int_{t_{i-1}}^{t_i} y(t)dt$; U^* is a vector of length 28 whose i^{th} element, u_i^*, is the PET reconstructed activity in the blood region of interest in the ith time interval; Y^* is a vector of length
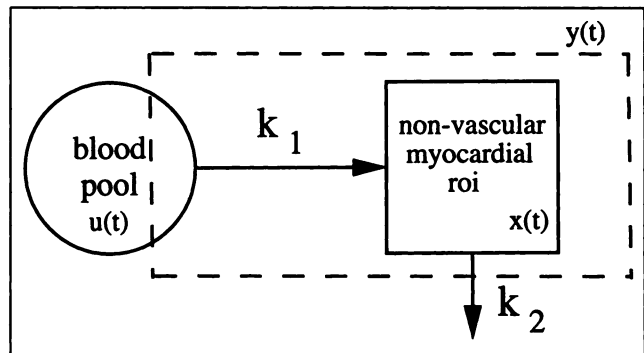

FIGURE 2. Two-compartment model of ^{82}Rb kinetics. Rubidium-82 in the blood pool is taken up in the nonvascular myocardium at a rate of k_1 min^{-1}, and washes out at a rate k_2 min^{-1}. Measurements y(t) include a vascular and a nonvascular component.
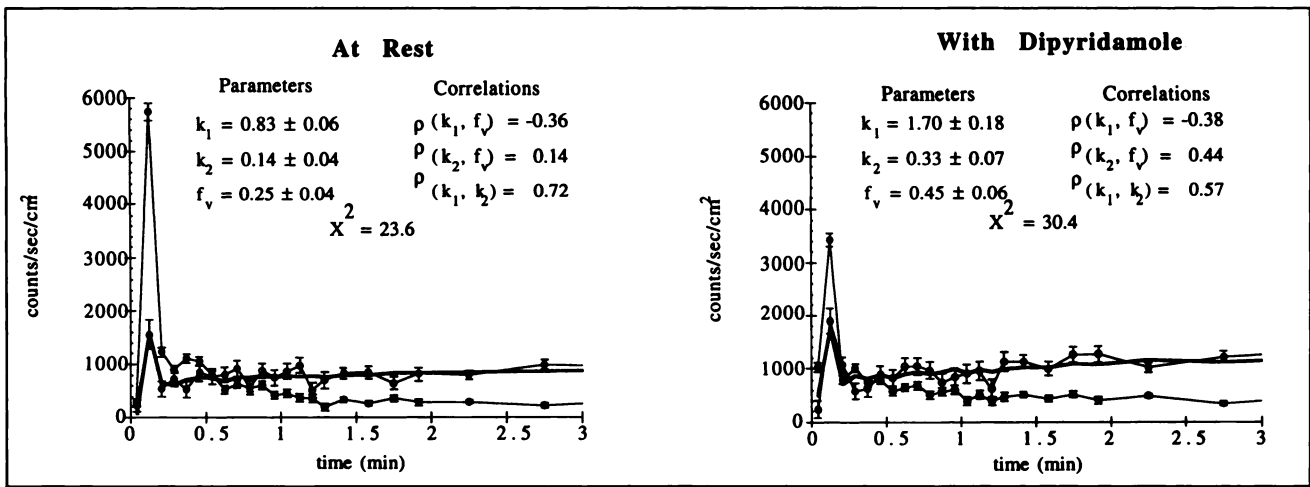
FIGURE 3. Sample data and model fit. Data from the blood pool (filled circles) and a lateral wall myocardial region of interest C12 (open circles) are displayed along with the model prediction for the fitted parameters. These data are from the rest and stress states for Dog 2 in the third week. The time axis has been truncated at 3 min to make it easier to see the fit in the first half minute. The number of degrees of freedom for the fit is 25. Parameter estimates and their standard deviations and the correlations between parameters are given.

28 whose i^{th} element, y_i^*, is the PET reconstructed activity in the myocardial ROI in the ith time interval; and Φ is the covariance matrix of the residual vector $(Y - Y^*)$ computed from Cov $[Y^*]$, Cov $[U^*]$, Cov $[Y^*, U^*]$, and the model parameters, (11).

Parameters k_1, k_2 and f_v were estimated for 11–14 circular ROIs, diameter 8 mm, in the myocardium. Estimates of parameters and of their uncertainties were obtained using algorithms previously described $(11,12)$. An example of the data $(u_i^*$ and y_i^*, $i = 1, \ldots, 28)$ and the fitted curve obtained with the model is shown in Figure 3.

Region of Interest Placement. Placement of myocardial ROIs was based on gated data acquired 100–420 sec after injection. Regions shown in Figure 4 were numbered in clockwise order starting in the septum and finishing in the lateral wall. Each 8-mm diameter circle is placed endocardially toward the left ventricular blood pool, and not to extend beyond the epicardial edge. Blood data $(u^*(t))$ were obtained from larger (10 mm or 15 mm) circular

ROIs in the left ventricle cavity. Guidelines for placing the blood pool region were determined by an investigation described in the Appendix. For data taken at the same PET position, the same regions were used to the extent that was reasonable. ROI counts and their covariances were evaluated directly from sinogram data using the method described by Huesman (13).

Heart Motion and Gating. Data were gated with two gates timed to real time EKG measurements. Kinetic parameter fits were separately determined for the gated data and the ungated data (that is, two gates combined). Often the statistics were inadequate to obtain a good fit for the single-gate data. Where the fits were acceptable, there was good agreement between the parameter estimates obtained both ways. For that reason, we have reported only the ungated results here.

The effect of heart motion is complex and quite different from other blurring effects such as positron range and crystal width, particularly with respect to symmetry. This is illustrated in Figure 5, where images from a 1985 dog study show the myocardial emissions from an injection of [18]FDG in two of eight gates. In this transverse slice, motion varies spatially along the heart wall, with most of the movement occurring in the vicinity of the apex. It should be noted that there is probably also motion in and out of
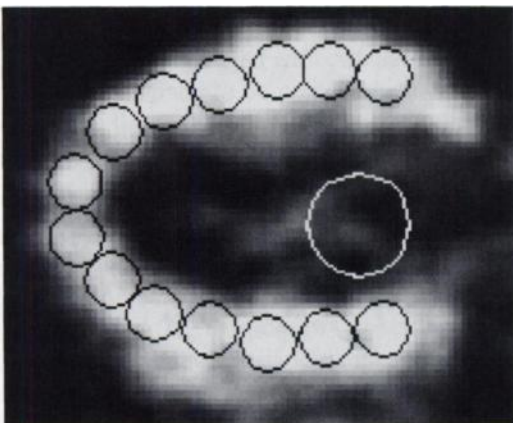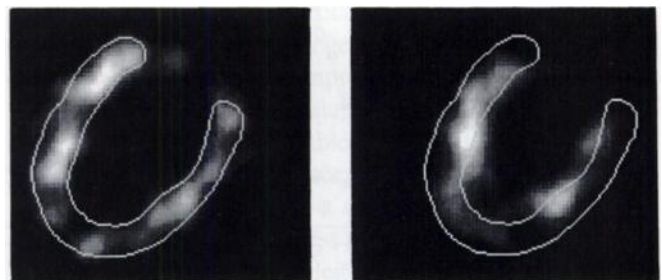

FIGURE 4. Regions of interest. A string of circular regions of interest, 8 mm in diameter, were placed in the myocardium of each transverse slice. Region C1 is at the lower right, in the septum, and the numbering continues clockwise to Region C14 in the lateral wall at the upper right. A larger ROI was placed in the left ventricular cavity to obtain blood pool data.

FIGURE 5. Gated data collection. Fluorine-18-FDG emissions from a gated dog heart study are shown for two of eight gates. The image on the left shows the left ventricular wall fully extended (end diastole), while the image on the right shows the contracted position. The same outline is drawn on both images to facilitate comparison.

FIGURE 6. Sample plots. Region-by-region plots show the parameter estimates for each small circular ROI, along with error bars representing estimates of the standard deviation. Summary box and whiskers plots provide a compact display of the distribution of parameter estimates among the 14 ROIs. The box delineates the inter-quartile range, while the whiskers give an indication of the range. Extreme values (defined in the text) are shown with circular markers.

a) Region by Region Plot   b) Summary Box Plot
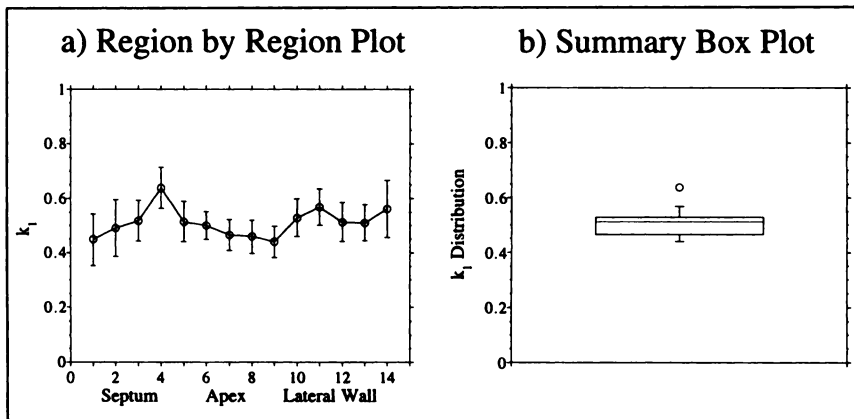
this fixed plane. Displacement inward from the epicardial wall is less than displacement inward from the endocardial wall. In the septum and lateral wall, ROIs drawn slightly in from the epicardial wall and leaning into the left ventricle blood pool are less susceptible to missed counts (myocardial recovery fraction less than one) than regions near the apex. The effect in terms of bias in apical k_1 estimates is discussed below. Total (ungated) counts are dominated by the extended (end diastole) position.

RESULTS

Kinetic parameters obtained in these experiments are displayed in Figures 6–12 and are discussed below. There are two kinds of plots, as illustrated in Figure 6. Region-by-region plots (Fig. 6a) show the parameter estimate for each of the 14 circular ROIs. Error bars are the estimated standard deviations based on inverting the second deriva-
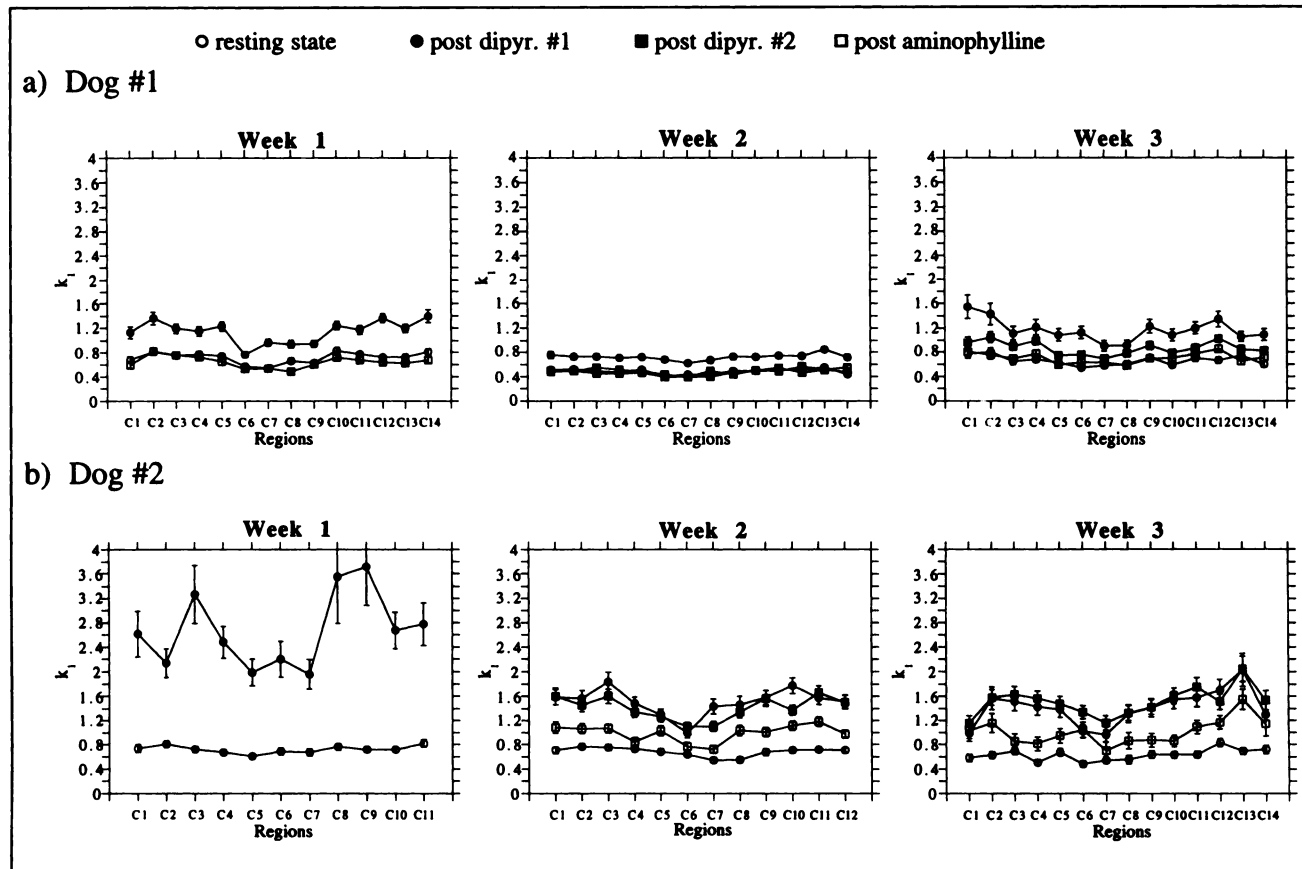

○ resting state   ● post dipyr. #1   ■ post dipyr. #2   □ post aminophylline

a) Dog #1

b) Dog #2

FIGURE 7. Region-by-region estimates of k_1 at three PET positions at rest. The protocol called for three rest-state bolus injections at three different PET positions (Rb1, Rb2 and Rb3) and a fourth injection (Rb6) repeating one of the three positions. For each of these injections, the k_1 estimate and its standard deviation are shown for each circular ROI in the myocardium. Filled markers represent k_1 estimates for injections at the bed position which was repeated (position 3), while open circles represent estimates from injections at other positions.
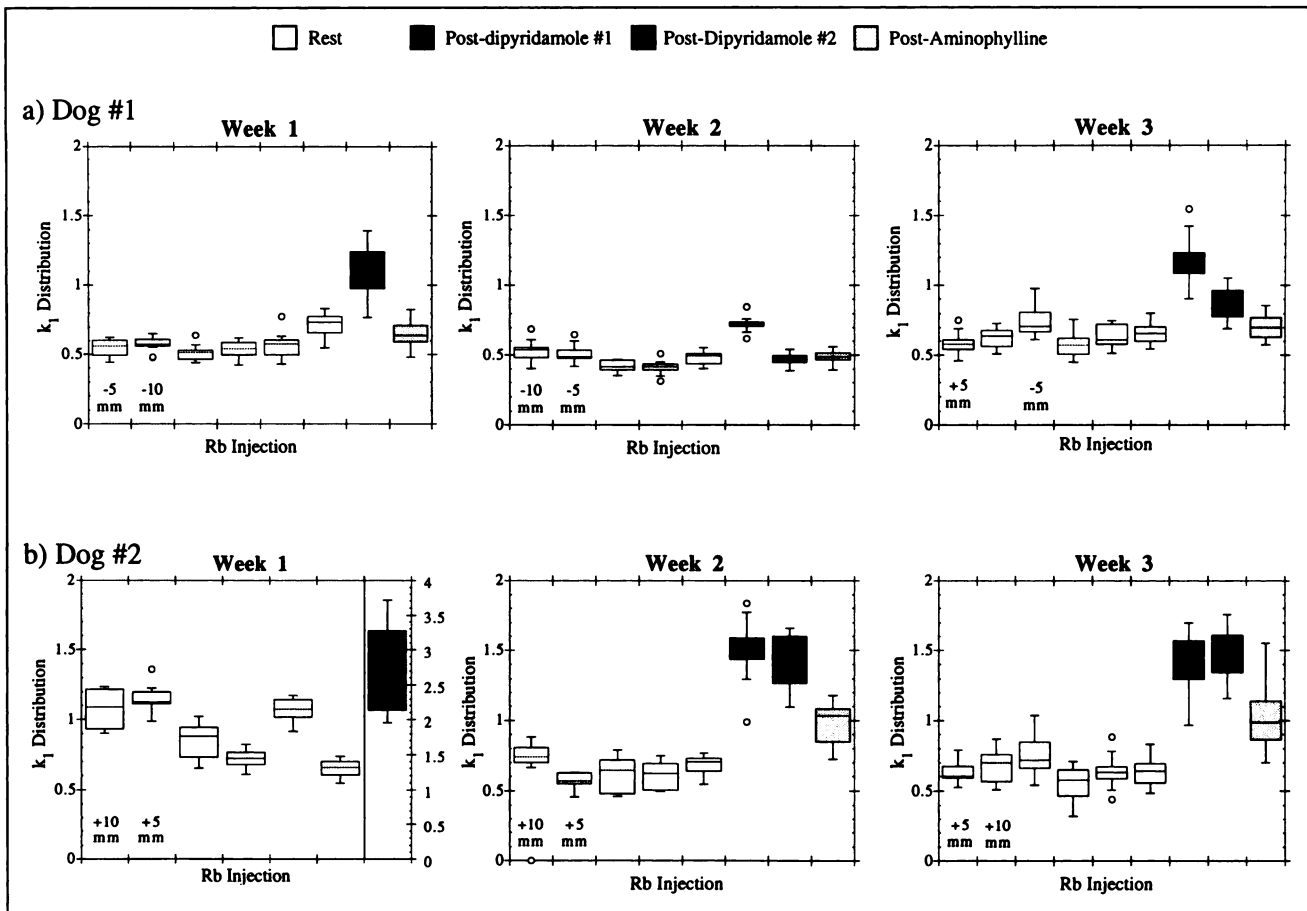
FIGURE 8. Summary plots of k_1. The distribution of k_1 (uptake, min^{-1}) for each ^{82}Rb injection of the study is shown with a box and whiskers plot. Each week, all injections except for two were imaged at the same PET position. The two exceptions are labeled with their displacement from the third position (± 5 mm, ± 10 mm).

tive of the criterion function. Box and whiskers plots (*14*) such as Figure 6b summarize the distribution of parameter estimates among the 14 ROIs. The top and bottom of the box are the upper and lower quartiles. Whiskers delineate the maximum and minimum, except for extreme values which are separately indicated with circular markers. (Extreme values are defined to be points which are at least a distance of 1.5 times the interquartile range beyond the interquartile range). The middle dotted bar marks the median k_1 value.

k_1 Estimates at the Three Different PET Positions

The protocol called for three kinetic PET datasets (Rb1, Rb2 and Rb3) to be measured in distinct lateral PET slices separated by 5 mm. The purpose of this sequence of measurements was to determine if variations observed from one week to the next might simply reflect the fact that the position of the PET slice had changed slightly. A fourth rest-state bolus injection (Rb6) generated a second dataset at one of the three positions. In Figure 7 the k_1 estimates are shown for all four injections for both dogs in each of three weeks. Slices in all weeks cover roughly the same region of the myocardium although the smaller length around the myocardium in Dog 2 in Week 2 suggests that

those slices were slightly more apical. The k_1 estimates for each dog are displayed with a separate plot for each of the 3 wk. The range of k_1 estimates for all regions in all weeks in all four rest-state bolus injections is [0.4 min^{-1}, 1.4 min^{-1}], with the first dog toward the lower end of the range (mean $= 0.6$ min^{-1}) and the second dog toward the higher end (mean $= 0.8$ min^{-1}).

Slice-to-slice differences in the same week reflect variation due to position and to temporal changes in the 10 min between injections. Differences between weeks reflect temporal variation over a longer period of time, as well as spatial variation due to the imprecise nature of cardiac slice location. The mean k_1 estimate for each slice (mean of k_1 in all regions) is about as variable between different slices in the same week as it is between slices imaged in different weeks. For Dog 1 there is a difference of 10%–20% between the largest and smallest mean among the four slices in each week. The overall means ($\pm$ s.d.) for Dog 1 for all three slices are 0.588 ± 0.101 min^{-1} (Week 1), 0.483 ± 0.070 min^{-1} (Week 2) and 0.655 ± 0.102 min^{-1} (Week 3). For Dog 2, these means are 0.949 ± 0.200 min^{-1} (Week 1), 0.655 ± 0.102 min^{-1} (Week 2) and 0.667 ± 0.111 min^{-1} (Week 3), with differences of 15%–50% between the largest
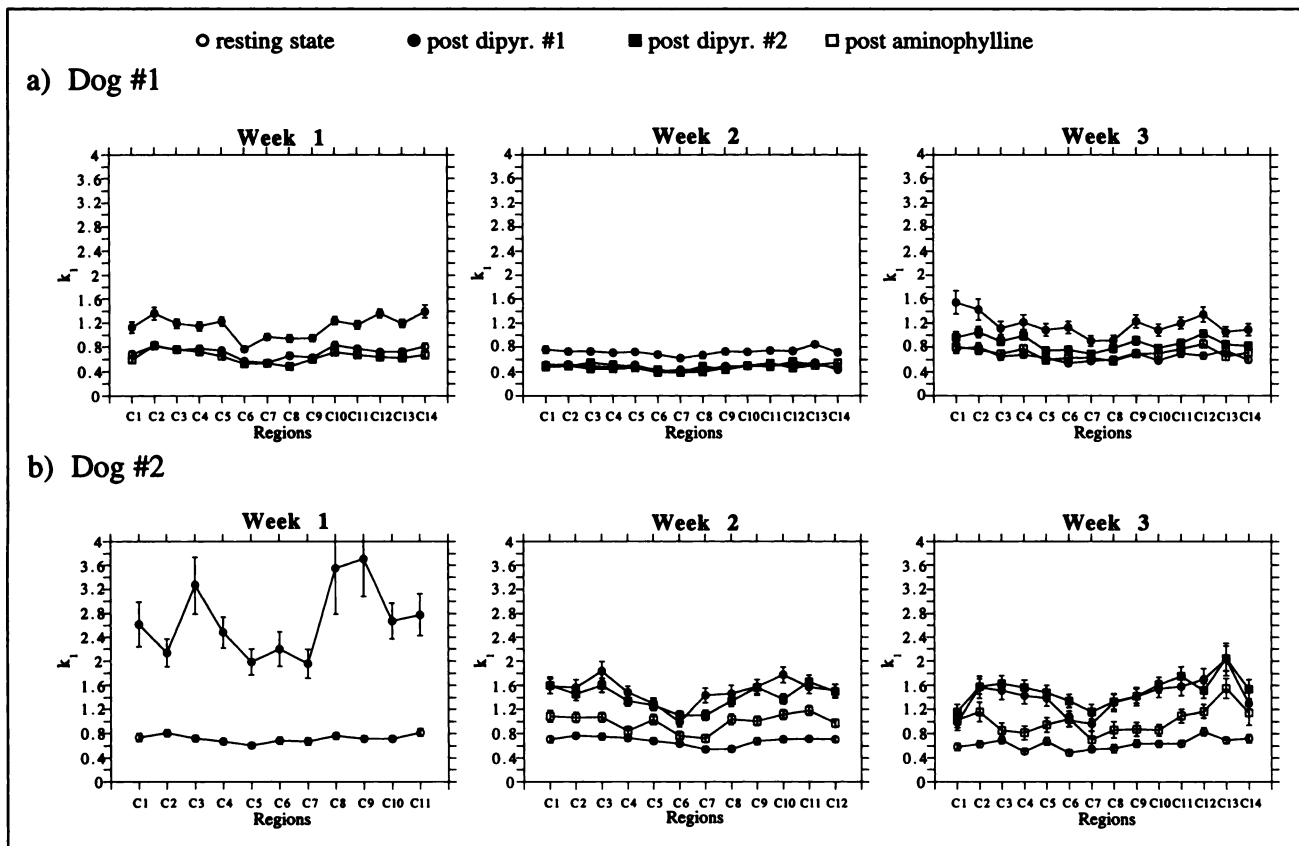
FIGURE 9. Region-by-region estimates of k_1 for the rest-dipyridamole sequence. Estimates of k_1 are shown for the rest bolus injection immediately preceding dipyridamole, two postdipyridamole injections and a postaminophylline (returned to rest) state. All data for a single dog in a particular week were collected at the same PET position.

and smallest mean among the four slices in 1 wk. The box and whiskers plots in Figure 8 summarize the distribution of k_1 for all injections in the study. Rest-state injections are shown with unfilled boxes.

k_1 Estimates at Rest and With Dipyridamole

The diagnostic utility of ^{82}Rb imaging of the myocardium rests on the ability to detect increases in uptake (k_1) corresponding to regional increases in blood flow. Dipyridam-

FIGURE 10. Spatial and temporal variation of k_1 in the resting state. Each plotted point is the mean of k_1 in one anatomical region for the four rest-state datasets on one date.

ole is infused over 5 min to induce vasodilation of myocardial blood vessels. This results in significant increases in blood flow in myocardial regions not affected by disease. In healthy subjects, it is expected that blood flow k_1 would increase in all regions. In each of the 3 wk, both dogs had a characteristic increase in k_1 following injection with dipyridamole, as seen in Figure 9 and in the summary plots of Figure 8. The minimum increase for all regions in all weeks was 34% of the resting value. The range of increase was 34%–108% for Dog 1 and 55%–194% for the last 2 wk with Dog 2. For the first week with Dog 2, the range was 163%–417%. The mean increases in k_1 over the myocardial regions for Dog 1 were 60% (Week 1), 50% (Week 2) and 77% (Week 3). For Dog 2, the mean increases were 313% (Week 1), 121% (Week 2) and 124% (Week 3).

In Weeks 2 and 3, a second rubidium injection was given after dipyridamole. For Dog 2, the second injection produced k_1 estimates very close to those of the first injection. For Dog 1, the situation is quite different. In Week 2, the k_1 estimates for the second injection are almost identical to those of the resting state. In Week 3, they are midway between the first injection and the resting state. These results raised questions about the persistence of the effect of dipyridamole which are being explored in another study.

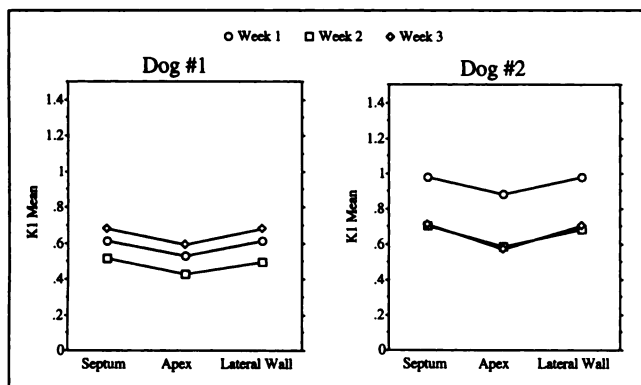The protocol called for ^{82}Rb to be injected shortly after

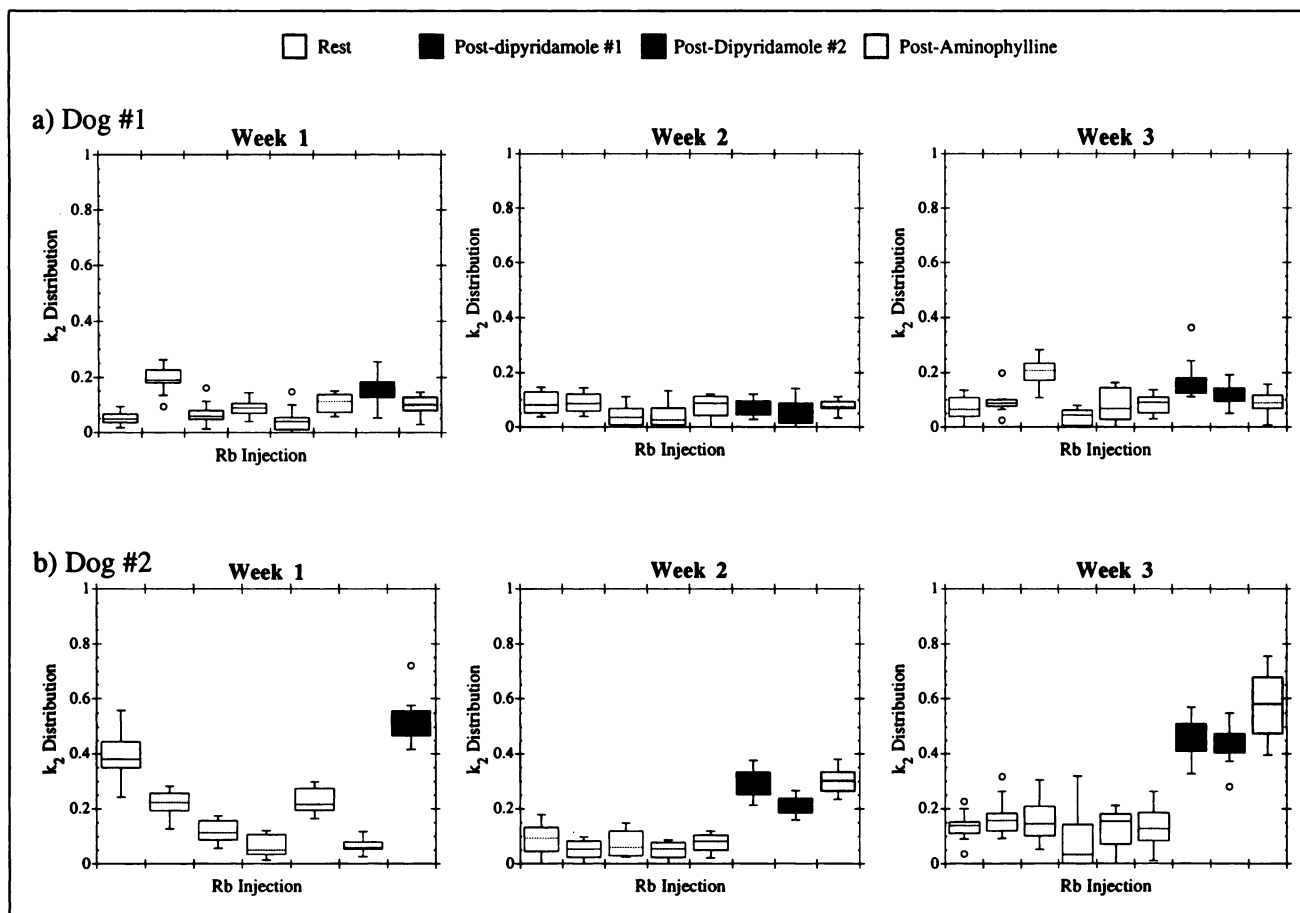Rest ☐   Post-dipyridamole #1 ■   Post-Dipyridamole #2 ■   Post-Aminophylline ☐

FIGURE 11. Summary plots of k_2.

the 5-min injection of dipyridamole. In Week 1, the time interval between the start of the dipyridamole injection and the ^{82}Rb injection was 10 min for Dog 1 and 22 min for Dog 2. In Weeks 2 and 3, the two postdipyridamole rubidium injections were given 6 ± 2 min and 15 ± 2 min, respectively, after the start of the dipyridamole injection. The dose varied somewhat (0.8–1.8 mg/kg) because each injection of dipyridamole was halted when a significant drop in blood pressure was observed. Dog 1 received doses 1.8, 1.6 and 1.2 mg/kg in Weeks 1, 2 and 3, respectively, while the doses for Dog 2 were 1.3, 0.8 and 0.8 mg/kg. Every injection of dipyridamole was accompanied by a drop in blood pressure. Heart rate was unchanged after dipyridamole in Dog 2 but dropped 20 bpm every week in Dog 1.

Comparison of Rest and Postaminophylline Estimates of k_1

Aminophylline is administered to counter the effect of dipyridamole. For Dog 1, the rest and postaminophylline k_1 values are essentially identical (Fig. 9, bottom row), with postaminophylline injections of ^{82}Rb given 14 min, 4 min and 10 min after the start of the aminophylline injection in Weeks 1, 2 and 3, respectively. For the second dog, the postaminophylline k_1 values are roughly halfway between the resting and dipyridamole states. These measurements

were taken 13 min (Week 2) and 40 min (Week 3) after the start of the aminophylline injection.

Spatial and Temporal Variation of k_1

Figure 10 shows the k_1 means over the four rest-state bolus injections in three anatomical regions: septum, apex and lateral wall. The data are separated by week. Overall, region-to-region variations are clearly less than week-to-week variation.

The most persistent spatial pattern is the slightly reduced k_1 values of the apex, at the left end of the transverse slice. Although Figure 10 displays values for the rest state only, this pattern is a feature in all states and all injections. Most likely, this is an artifact of partial volume or motion effects. As discussed earlier, heart motion in the transverse slice is much greater in the apical regions than in the septal or lateral wall regions. Potentially, this could explain the lower k_1 values; however, the effect persists even if gated data are used. This suggests that heart motion is not the only relevant factor. Since the parameter bias is very consistent, it is clear we could compensate for it. Larger ROIs in the apex, stretching further into the left ventricular blood pool would capture more of the myocardial emissions. Alternatively, a variable myocardial recovery fraction could be introduced into the model. Since the bias is quite
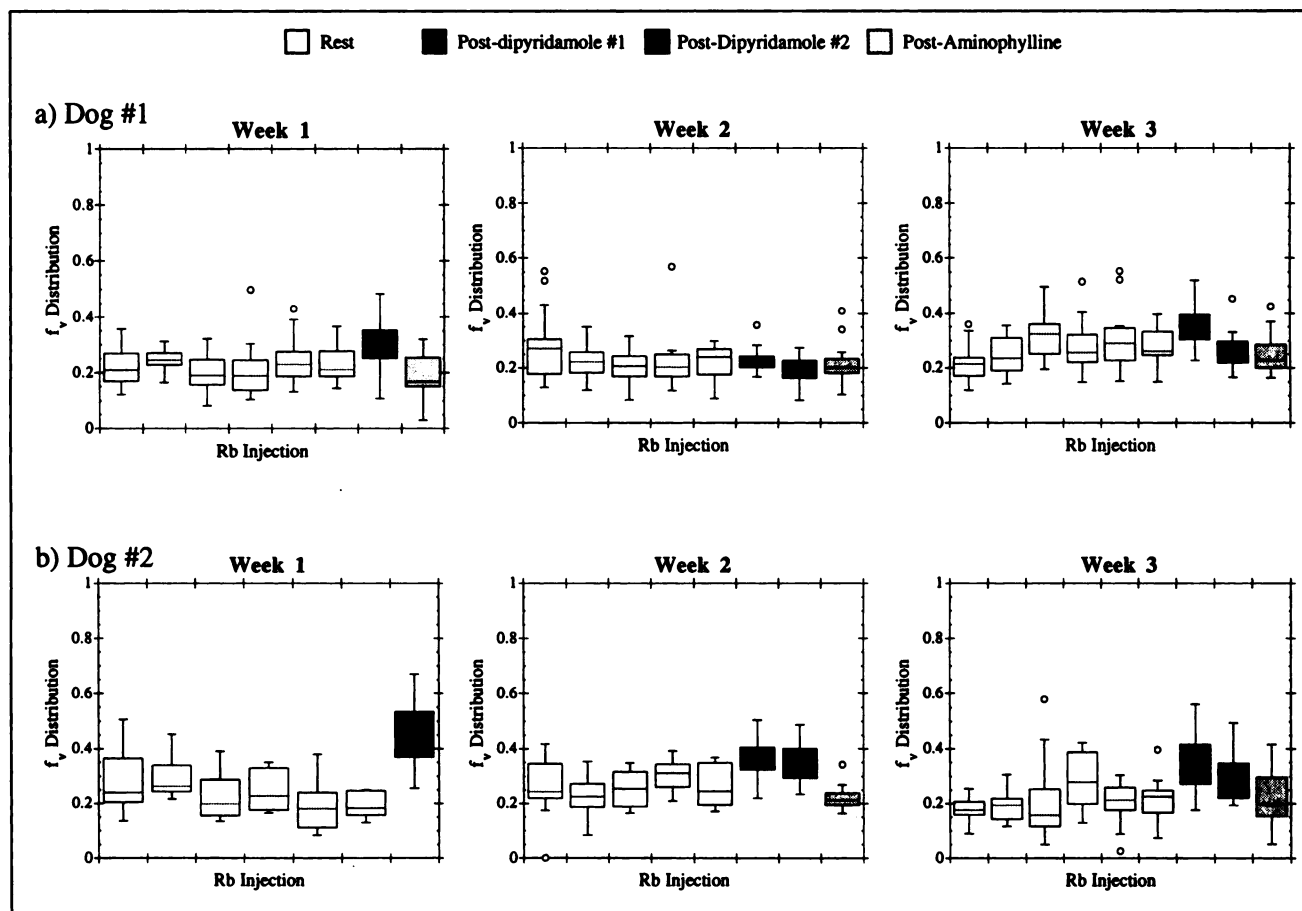
□ Rest   ■ Post-dipyridamole #1   ■ Post-Dipyridamole #2   □ Post-Aminophylline

a) Dog #1

FIGURE 12. Summary plots of f_v.

small, and its cause is not well specified, we have chosen to simply illustrate it.

Vascular Fraction and Washout Rate

Because the [82]Rb uptake rate k_1 increases with blood flow, it is the parameter of greatest interest and we have focused our attention there. Above, we examined the values of k_1 in the small circular ROIs around the heart wall to assess the variation in time and space relative to some of the controlled variations set forth in the experimental design. To complete the picture, we include summary plots of the remaining two parameters, k_2 and f_v, for the eight to nine studies with each dog in each of 3 wk. Figures 11 and 12 show the mean and sample standard deviation of k_2 and f_v, respectively, for the 11–14 ROIs for each injection of [82]Rb.

The vascular fraction f_v takes into account both actual vasculature in the myocardium, spillover of blood counts from external sources (mainly the left ventricular cavity), and interstitial sources which are similar to vascular emissions. Spillover results from imperfect resolution of the PET data and also from heart motion and placement of the ROI in the myocardium. Region placement was always endocardial to avoid spillover from outside (lung and right ventricle).

DISCUSSION

A sequence of [82]Rb kinetic PET studies was repeated three times to assess the variability and reproducibility of the resulting estimates of three kinetic parameters: k_1 (uptake rate), k_2 (washout rate) and f_v (vascular fraction). The sequence included data acquisitions during rest, dipyridamole and returned-to-rest states. It was determined that the spatial (slice-to-slice, region-to-region) and temporal (week-to-week, injection-to-injection) variation in the rest-state k_1 was small in comparison to the functional increase in k_1 accompanying dipyridamole. This holds true not only on average, but also in the individual small ROIs. Differences in k_1 between the two animals may be related to their different build and heart rate (noted in Methods section), but there is no way to confirm this without a larger investigation.

For each dog, the actual values of k_1 are very close in 2 of 3 wk, but in 1 wk, the postdipyridamole values are quite different both in magnitude and variability across regions. The first week study of Dog 2 was subject to delays which may have affected the physiological state of the animal, but there were no observed or measured variables in the second week which could account for the different response observed in Dog 1. This suggests that additional significant
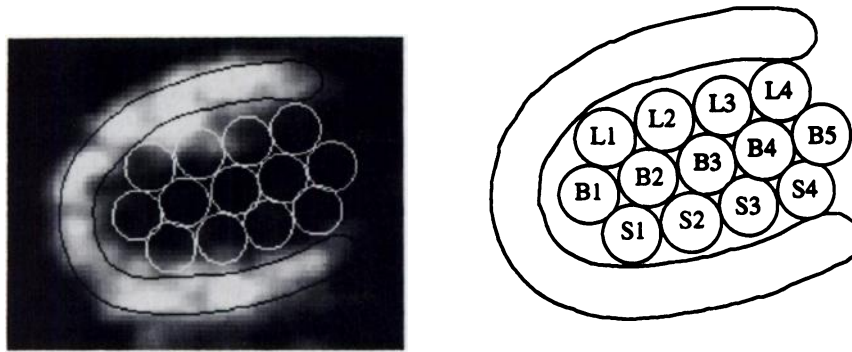
FIGURE 13. Thirteen 10-mm diameter circular ROIs were placed in the left ventricular cavity to determine the best placement for a blood ROI. Labels for each region are shown at right.

experimental or physiological factors exist which can affect ^{82}Rb kinetic behavior.

The reduced k_1 estimates for the second postdipyridamole injection in Dog 1 raise a question about the duration of the effect of dipyridamole. They suggest that the effect was already wearing off 15 min after the dipyridamole injection. This is not true of Dog 2, where the second injection shows an effect at least as strong as the first. Differences in the magnitude and consistency of the post-dipyridamole k_1 values do not appear to be related to the dose of dipyridamole or to the timing of the rubidium injections. These variables were not intentionally varied in the protocol.

There have been numerous studies of the effects of di-pyridamole on canine heart physiology using catheters or electromagnetic flow meters to monitor blood flow. West et al. (15) observed that an increase in coronary blood flow with a peak of 28%-350% was sustained for 10-30 min in 14

mongrel dogs following intravenous injection of dipyridam-ole. Heart rate decreased by 5-35 bpm in 12 of the 14 dogs, which is statistically significant ($p < 0.05$) by a paired t-test (West reports a higher p-value which is not significant, based on an unpaired test). Saito also recorded a decrease in the mean heart rate for 20 normal mongrel dogs (16). Our results are consistent with these findings.

Since the dipyridamole results for Dog 1 suggested that the effect of dipyridamole was rapidly wearing off, the observed return to the resting state following injection of aminophylline may have little to do with the aminophyl-line. With Dog 2, it appears that aminophylline may counter the effect of dipyridamole to some extent, but does not negate that effect completely. This agrees with obser-vations of Brown et al. (17) in which aminophylline was administered to counter dipyridamole in coronary artery disease patients.

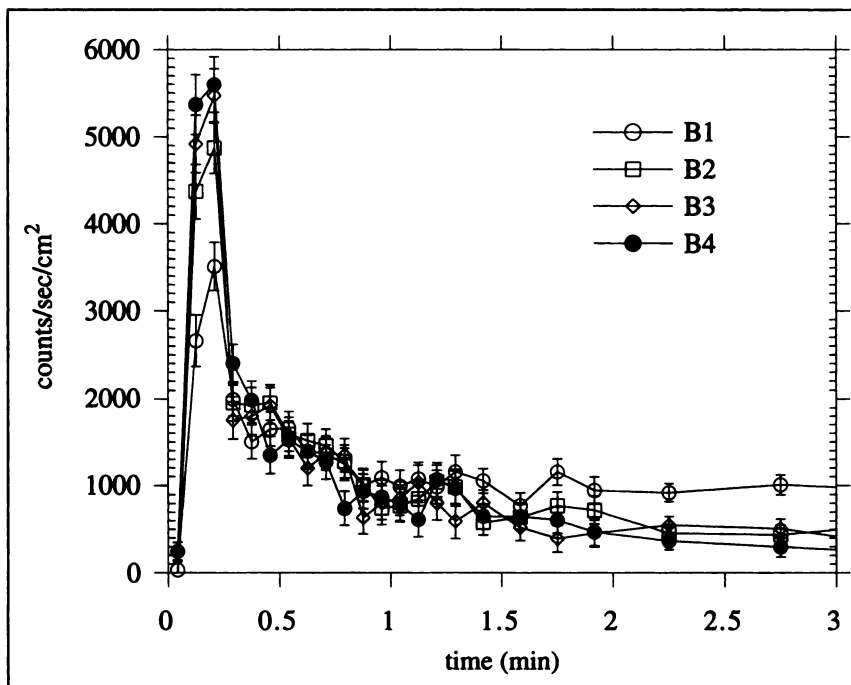Although many of the questions which motivated this

FIGURE 14. Time-activity curves for 10-mm blood regions. Lower peak and higher tail values reflect spillover from the myocardium. ROIs in the left ventricular blood pool give a truer representation of blood levels if placed nearer to the valve end of the transverse slice.

study were answered, the results forced us to reformulate some and to ask new questions. A new series of studies was designed to address many of the issues raised in this report and to test the major findings with a larger sample. The results will be included in a future report.

APPENDIX

Blood Pool Regions of Interest

The effect of location of the blood pool ROI was investigated by considering a cluster of thirteen 10-mm diameter circular regions covering the left ventricular cavity. Figure 13 shows the location of the regions in a particular heart. Time-activity curves for these regions were compared. Regions least affected by spillover effects have higher peak values and lower tail values (Fig. 14). More regions were affected by spillover in the studies with dipyridamole than in the resting state. Region B4 was consistently better than other regions when both rest and dipyridamole states were examined. In general, the shaded regions in Figure 13 gave good results. This is consistent with the gated emission study in Figure 5 which showed the same region to be least affected by heart motion. Circular ROIs centered in this area were used for the analysis reported in this paper.

ACKNOWLEDGMENTS

REFERENCES

1. Beanlands R, Schwaiger M. Cardiac applications of position-emission tomography. *Curr Opin Radiology* 1991;3:817–827.
2. Go RT, Marwick TH, MacIntyre WJ, Saha GB, Neumann DR, Simpfendorfer CC. A prospective comparison of rubidium-82 PET and thallium-201 SPECT myocardial perfusion imaging utilizing a single dipyridamole stress in the diagnosis of coronary artery disease. *J Nucl Med* 1990;31:1899–1905.
3. Budinger TF, Derenzo SE, Huesman RH, Sherman LG, Moyer BR, Yano Y. Quantitative myocardial flow-extraction data using gated ECT. *J Nucl Med* 1980;21:P16.
4. Hicks K, Ganti G, Mullani N, Gould KL. Automated quantitation of three-dimensional cardiac positron emission tomography for routine clinical use. *J Nucl Med* 1989;30:1787–1797.
5. Herrero P, Markham J, Shelton ME, Bergmann SR. Implementation and evaluation of a two-compartment model for quantification of myocardial perfusion with rubidium-82 and positron emission tomography. *Circ Res* 1992;70:496–507.
6. Yano Y, Budinger TF, Cahoon JL, Huesman RH. An automated microprocessor-controlled Rb-82 generator for positron emission tomography studies. In: Knapp FF, Butler TA, eds. *Radionuclide generators*. Washington, DC: American Chemical Society; 1982:97–122.
7. Derenzo SE, Huesman RH, Cahoon JL, et al. A positron tomograph with 600 BGO crystals and 2.6 mm resolution. *IEEE Trans Nucl Sci* 1988;35: 659–664.
8. Derenzo SE, Huesman RH, Cahoon JL, et al. Initial results from the Donner 600 crystal positron tomograph. *IEEE Trans Nucl Sci* 1987;34:321–325.
9. Haber SF, Derenzo SE, Uber D. Application of mathematical removal of positron range blurring in positron emission tomography. *IEEE Trans Nucl Sci* 1990;37:1293–1299.
10. Huesman RH, Derenzo SE, Cahoon JL, et al. Orbiting transmission source for positron tomography. *IEEE Trans Nucl Sci* 1988;35:735–739.
11. Huesman RH, Mazoyer BM. Kinetic data analysis with a noisy input function. *Phys Med Biology* 1987;32:1569–1579.
12. Coxson PG, Salmeron EM, Huesman RH, Mazoyer BM. Simulation of compartmental models for kinetic data from a positron emission tomograph. *Comput Meth Prog Biomed* 1992;37:205–214.
13. Huesman RH. A new fast algorithm for the evaluation of regions of interest and statistical uncertainty in computed tomography. *Phys Med Biol* 1984; 29:543–552.
14. Abelbeck Software. *Kaleidagraph*, version 3, 1993.
15. West JW, Bellet S, Manzoli UC, Muller OF. Effects of Persantin (RA8), a new coronary vasodilator, on coronary blood flow and cardiac dynamics in the dog. *Circulation Res* 1962;10:35–44.
16. Saito D. Effect of coronary vasodilators on cardiac dynamics of the normal dog and the dog with experimental coronary sclerosis. *Jpn Circulation J* (English edition) 1976;40:363–397.
17. Brown BG, Josephson MA, Petersen RB, et al. Intravenous dipyridamole combined with isometric handgrip for near maximal acute increase in coronary flow in patients with coronary artery disease. *Am J Cardiol* 1981;48: 1077–1085.